Cosmic abundance of elements & isotopes

data sources:

tangible: samples can be directly handeled

intangible: spectroscopy, remote sensing, or considerations from theor. astrophysics

bulk of radiation from stars originates in surface layers or "atmosphere" of stars —> photosphere

Table 3.1. *Data sources and methods for cosmic abundances*

Data sources		
	Tangible:	Intangible:
Earth:	atmosphere oceans crust	Earth: mantle core
	Astrophysical objects:	
Moon (Apollo meteorites) Mars (meteorites) Asteroids (meteorites) Comets (dust) Circum-/interstellar dust (meteorites).		Sun, planets, comets, stars, PN, SNR, H II regions, ISM, galaxies, intra-cluster gas (X-r), QSOs, intervening gas.
Space plasmas:	Ionosphere, magnetosphere Solar wind Cosmic rays	
Methods		
Chem. analysis Mass spectrometry Electron microscopy Optical microscopy X-ray diffraction Neutron activation, X-r fluorescence spectr., Ion + electron microprobe ICP-MS Proton probe (PIXE) Balloon and space-borne	for trace species nucl. em./plastic ion counters	Seismic methods Radar mapping Thermal mapping Spectrum analysis (abs. or em. lines) from γ-r to radio. Deductions from stellar structure and evolution.

hot stars $T_{eff} > 10^4$ K

photo ionization of hydrogen atoms

$H^* + h\nu \rightarrow H^+ + e^-$

$\Rightarrow$ absorption in Lyman ($\lambda \leq 912$ Å)

Balmer ($\lambda \leq 3646$ Å)

Paschen ($\lambda \leq 8208$ Å) etc

continua

cooler stars (Sun $T_{eff} = 5780$ K):

photo detachment of negative hydrogen ions

$$H^- + h\nu \ (\geq 0{,}75\,eV) \rightarrow H + e^-$$

accurate abundance analysis of stellar absorption lines is an elaborate physical & numerical exercise

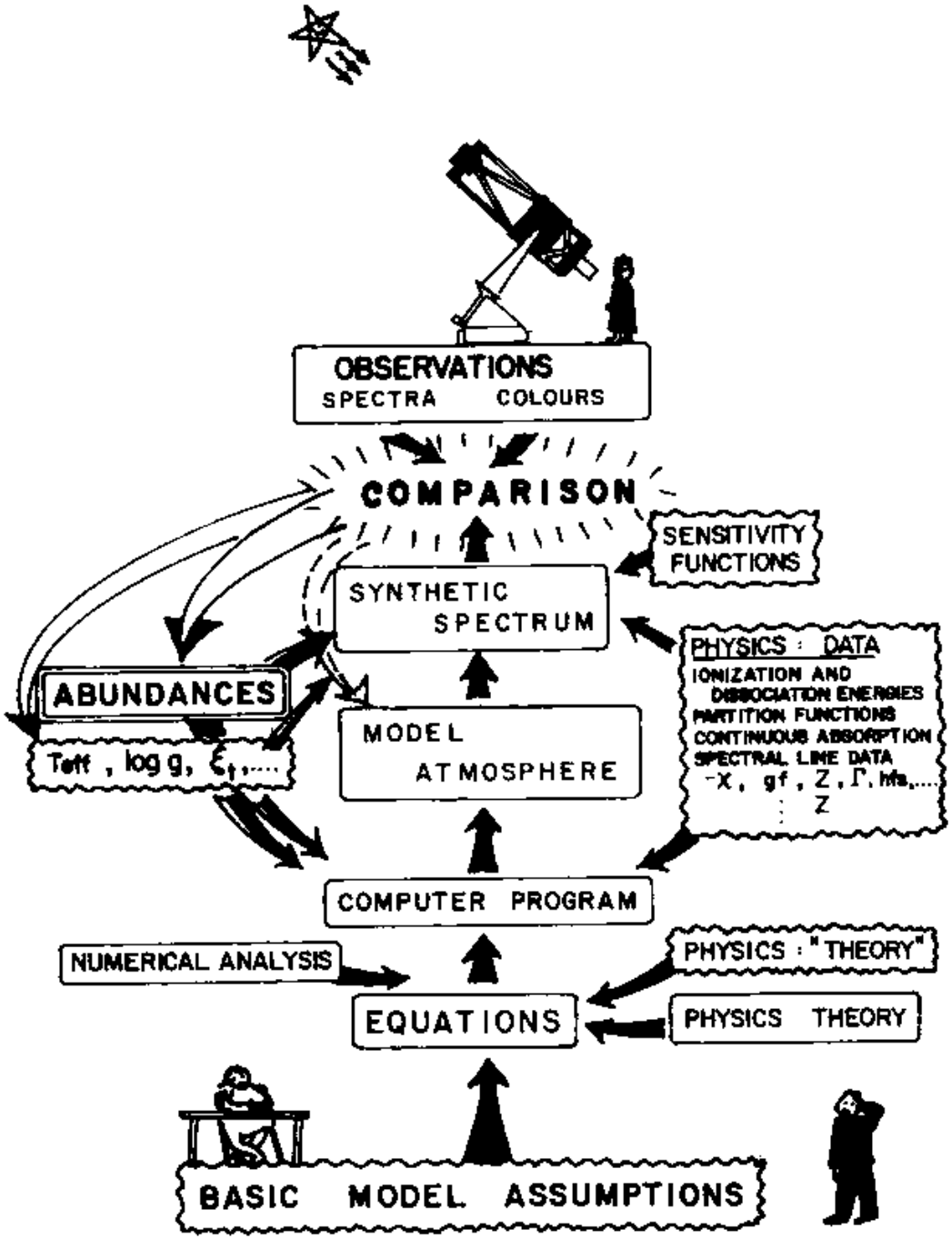

Fig. 3.3. Cartoon indicating steps in abundance analysis using model atmospheres. After Gustafsson (1980).

Abundances: main results

- solar abundance and local galactic abundance
  - photospheric absorption lines (Fraunhofer lines) provide element: hydrogen (M:H) ratios
  - emission lines from solar chromosphere: enhancement of elements with low first ionization potential (FIP effect)
  - Earth's crust, mantle, core influenced by "differentiation" gravitational separation in early

Table 3.4. *Solar abundances relative to* $\log N_{\mathrm{H}} = 12.00$*; meteoritic abundances relative to* $\log N_{\mathrm{Si}} = 7.51$

Element		Photospheric	Meteoritic	Element		Photospheric	Meteoritic
1	**H**	12.00		21	**Sc**	3.05	3.04
2	**He**	(10.93)		22	**Ti**	4.90	4.89
3	**Li**	1.05	3.25	23	**V**	4.00	3.97
4	**Be**	1.38	1.38	24	**Cr**	5.64	5.63
5	**B**	2.7	2.75	25	**Mn**	5.39	5.47
6	**C**	8.39		26	**Fe**	7.45	7.45
7	**N**	7.78		27	**Co**	4.92	4.86
8	**O**	8.66		28	**Ni**	6.23	6.19
9	**F**	4.6:	4.43	29	**Cu**	4.21	4.23
10	**Ne**	(7.84)		30	**Zn**	4.60	4.61
11	**Na**	6.17	6.27	37	**Rb**	2.6	2.33
12	**Mg**	7.53	7.53	38	**Sr**	2.92	2.88
13	**Al**	6.37	6.43	39	**Y**	2.21	2.17
14	**Si**	7.51	7.51	40	**Zr**	2.59	2.57
15	**P**	5.36	5.40	56	**Ba**	2.17	2.16
16	**S**	7.14	7.16	57	**La**	1.13	1.15
17	**Cl**	5.5:	5.23	58	**Ce**	1.58	1.58
18	**Ar**	(6.18)		60	**Nd**	1.45	1.43
19	**K**	5.08	5.06	63	**Eu**	0.52	0.49
20	**Ca**	6.31	6.29	90	**Th**		0.06

Data are from a review by Asplund, Grevesse and Sauval (2005). When two decimal places are given, the estimated error of photospheric abundances is of the order of ± 0.1; the meteoritic ones are usually somewhat more accurate. Values in brackets are based on solar wind and energetic particles normalized to oxygen; they are reasonably consistent with results from Galactic nebulae. The recent photospheric figures, largely based on 3D hydrodynamical simulations with non-LTE effects taken into account, correspond to a somewhat lower heavy-element content than was usually assumed earlier (e.g. Anders & Grevesse 1989): specifically, $(X, Y, Z, Z/X) \simeq (0.739, 0.249, 0.012, 0.0165)$, but the downward revision is hard to reconcile with helioseismology and has been disputed (e.g. Delahaye & Pinsonneault 2006). Solar System abundances, allowing for diffusion, are given and discussed by Lodders (2003); they are typically about 10 per cent higher.

molten phase of the planet

core (liquid/solid) $r = 3500$ km Fe, Ni, FeS

mantle $d = 2900$ km Fe, Mg silicate

solid crust 30–40 km thick, mainly of granite (Al-rich silicates)

10 km under oceans (Mg rich silicates)

- Meteorites: 3 types: stones, stony irons, iron

iron: metallic iron alloyed with Ni

stones: iron + FeS + iron magnesium silicates

most of meteorites result from breakup of asteroids, not subjected to differentiation (like Earth & Moon)

- abundances outside solar system

abundance variations in stars through 3 effects

- internal nuclear reactions followed by loss of the envelope or mixing to surface layers in advanced evolutionary stages

  white dwarfs classified according to spectral features DO(He^+), DB(He), DA(H)

- population effects

  stars are born with composition of ISM at time & place of formation

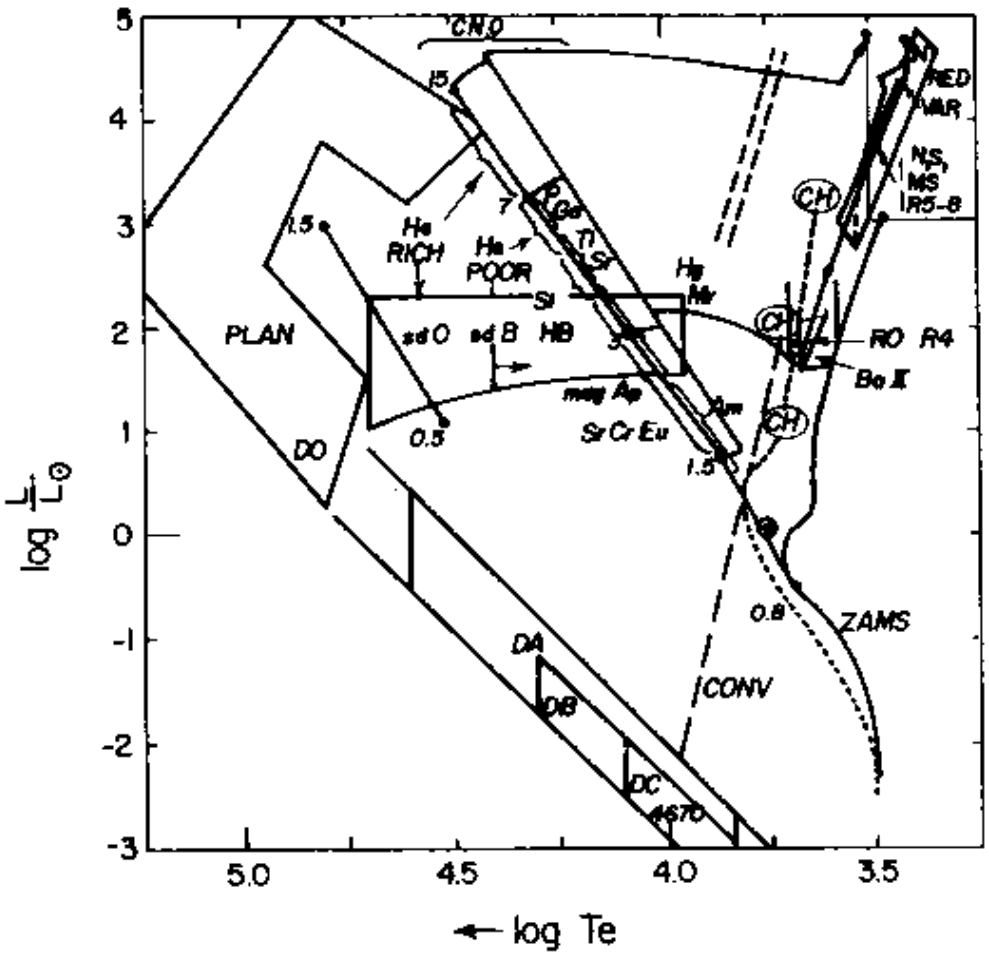

Fig. 3.37. Rough locations of chemically evolved and peculiar stars in the HR diagram. Full lines show the ZAMS with stellar masses indicated and evolutionary tracks for 0.8, 3 and 15 $M_\odot$, the helium main sequence (0.5 to 1.5 $M_\odot$), PN nucleus, horizontal-branch and white-dwarf regions. The dotted line shows a schematic main sequence and evolutionary track for Population II, while various dashed lines show roughly the Cepheid instability strip, the transition to surface convection zones and the helium-shell flashing locus for Population I. After Pagel (1977). Copyright by the IAU. Reproduced with kind permission from Kluwer Academic Publishers.

- stars with $T_{eff} \geq 8000$ K, called chemically peculiar (CP)

display extraordinare over- and underabundance of elements

→ gravitative settling & radiative levitation or selective accretion of gas, but not dust

- Metallicities & stellar populations

Walter Baade 1948: 2 stellar populations

Pop I + Pop II

Pop I: gas-rich galactic disk
young stars
metal rich

Pop II: center of galaxy, old stars
metal poor
high-velocity stars with elongated & inclined orbits

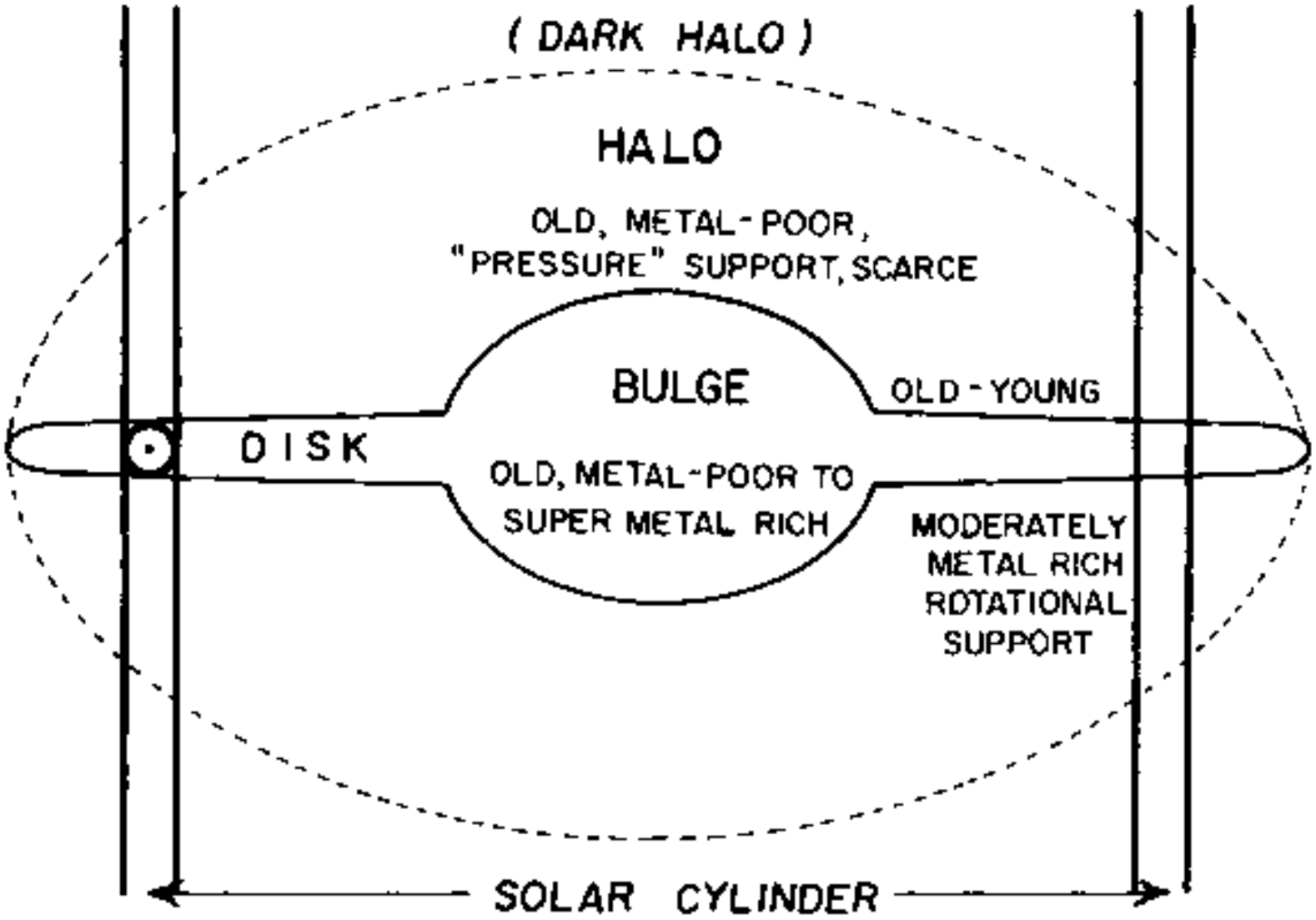

Fig. 3.38. Schematic cross-section through the Galaxy.

UV excess = [Fe/H] indicator of age

Galaxy formed by collapse on a free-fall time scale

first stars were formed in early stages of collapse with large orbital energies, i.e. large eccentricities & maximum heights

→ galactic halo

remaining gas cloud dissipated energy by collissions

→ galactic disk

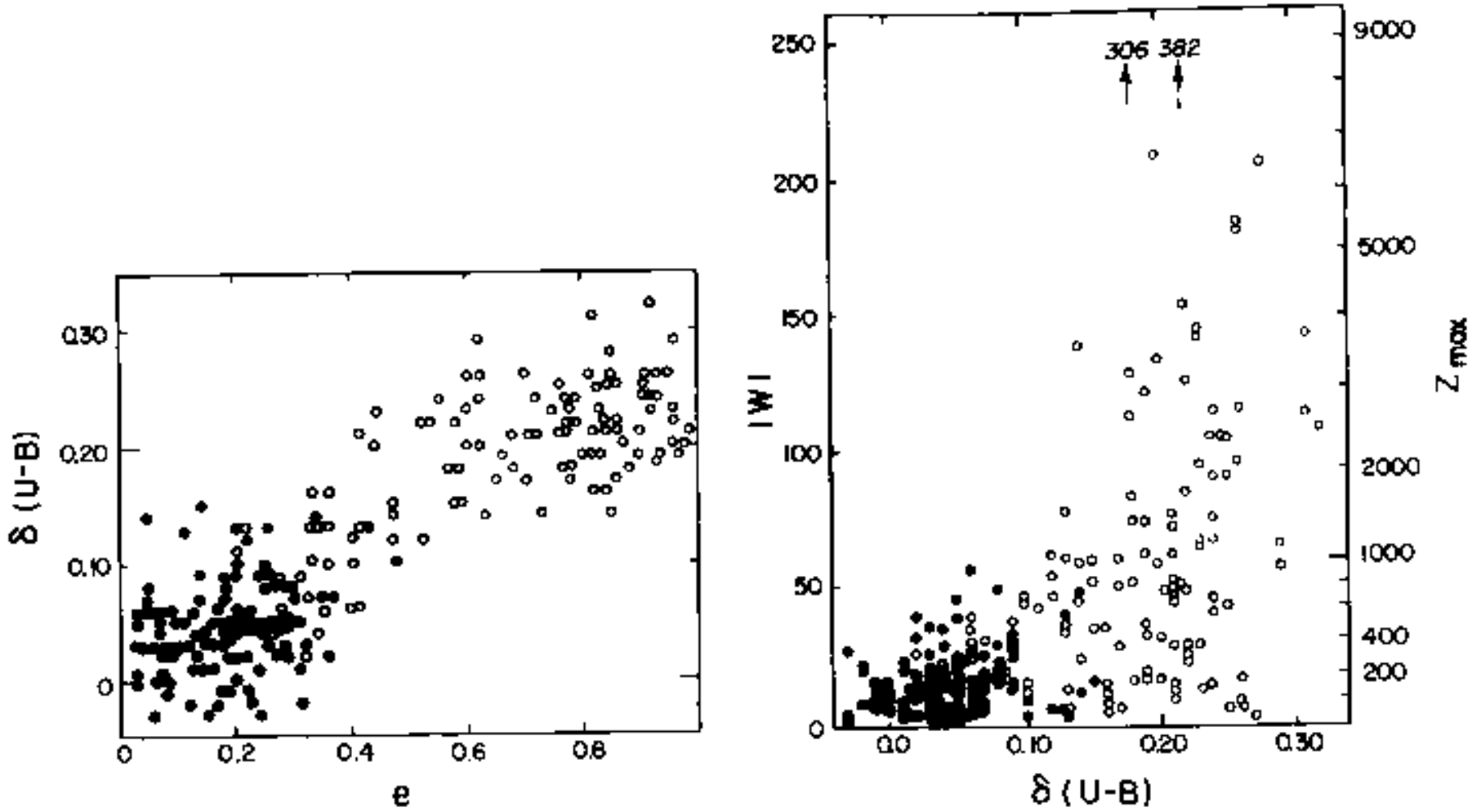

Fig. 3.39. Correlations between UV excess and stellar orbital eccentricity and velocity at right angles to the plane of the Milky Way. Adapted from Eggen, Lynden-Bell and Sandage (1962).

disk has two components:

thick disk: old stars

gas-rich thin disk, which may have accumulated over a long period

metallicity decreases with radius

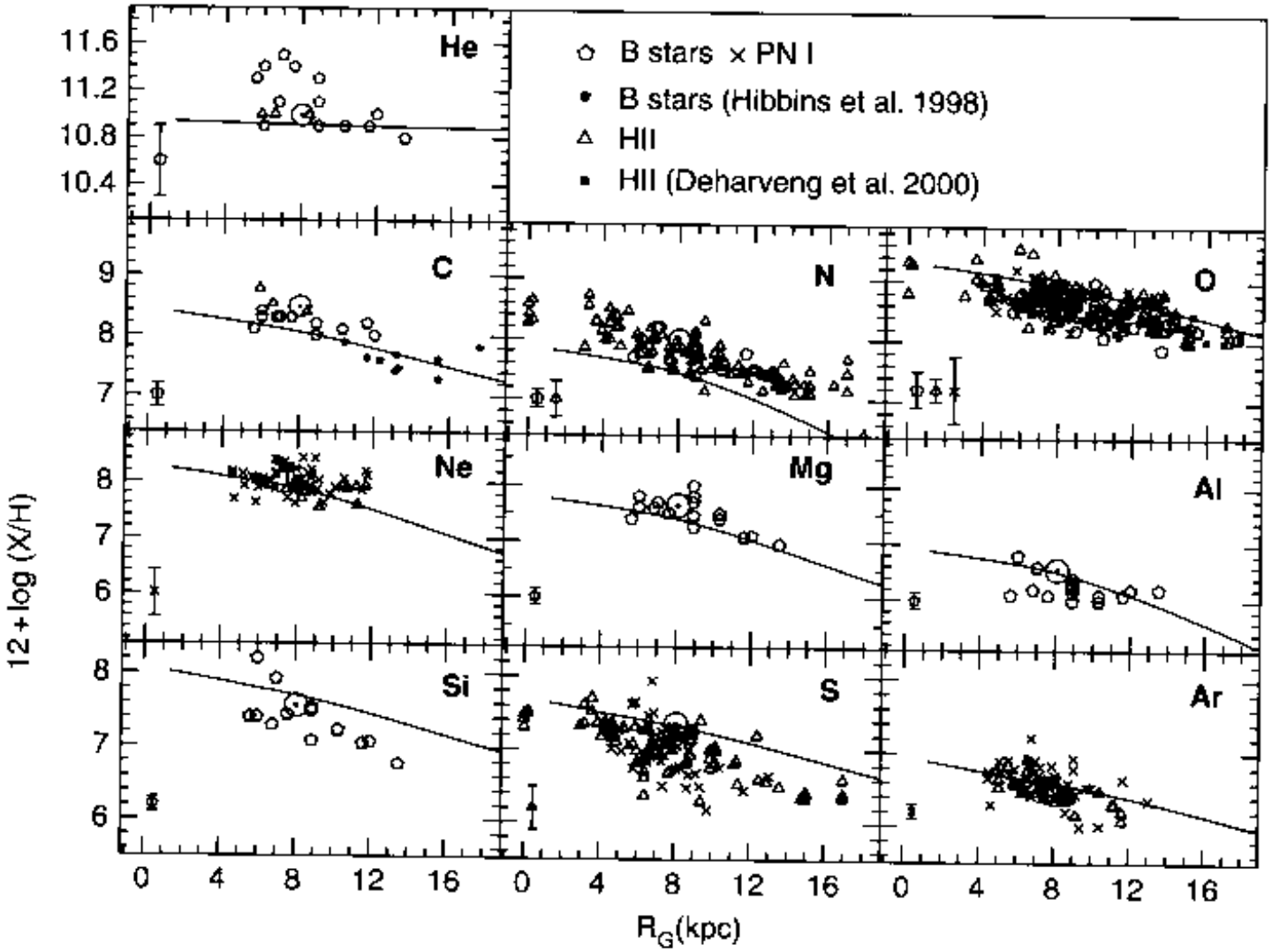

Fig. 3.40. Abundances in Galactic stars, H II regions and planetary nebulae, as a function of Galactocentric distance, with the Sun shown for comparison. After Hou, Prantzos and Boissier (2000). The curves show a model calculation by the authors; nitrogen is underproduced in the model because only massive stars were considered.

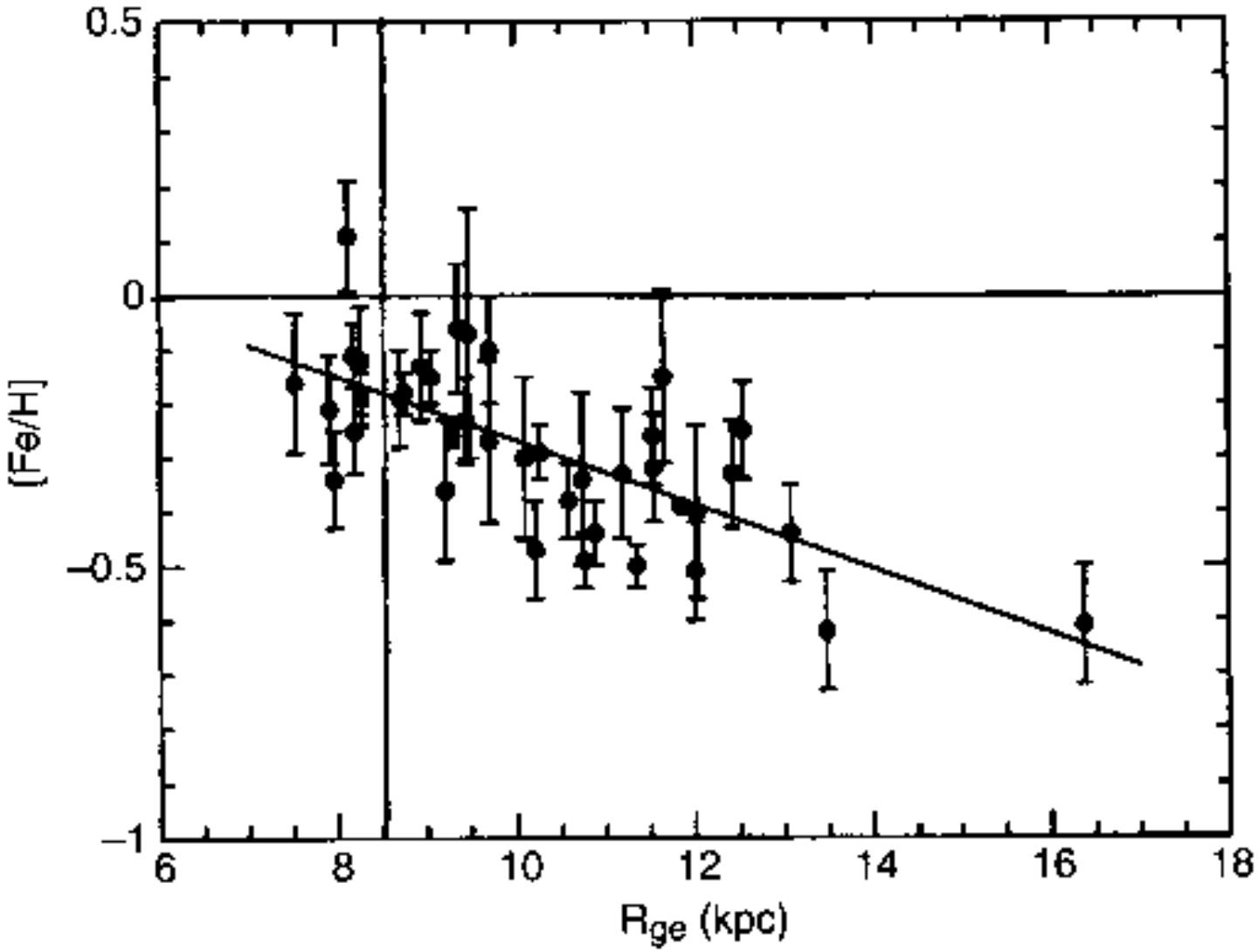

Fig. 3.41. Iron abundances in intermediate-age open Galactic clusters as a function of Galactocentric distance, with the Sun shown by the axes. The line corresponds to a gradient of $-0.06\,\mathrm{dex\,kpc^{-1}}$. Adapted from Friel *et al.* (2002).

- cold interstellar medium

ISM has complex structure

x-ray gas, warm ionized + neutral gas

H II regions ionized H

H I clouds neutral H + H_2

most elements of H I gas are depleted

rel. to sol. abundance

depletion decreases with condensation

temperature

→ these elements are ejected from stars

in the form of dust

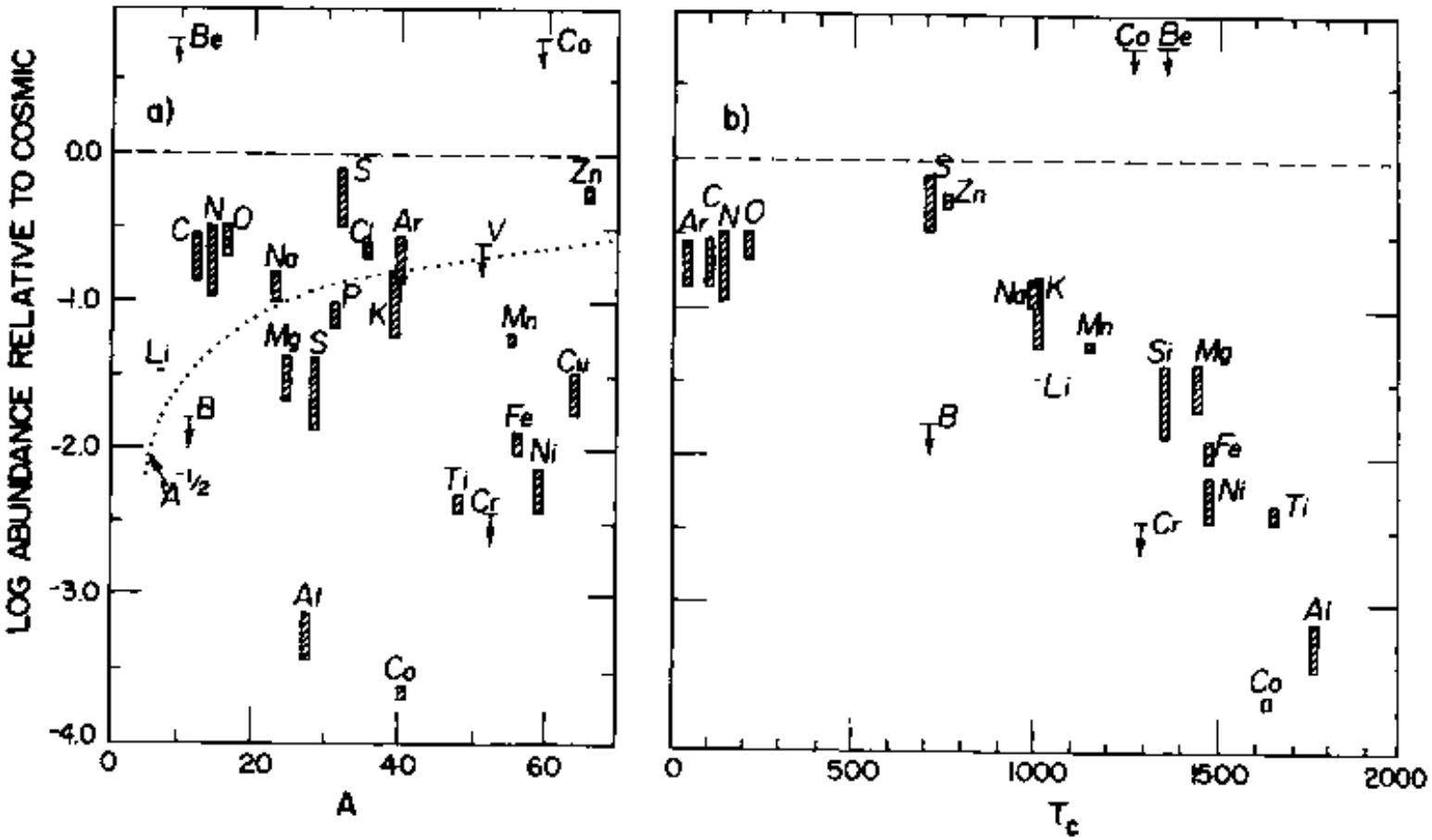

Fig. 3.42. Depletion below solar abundances of elements in the H I gas towards ζ Ophiuchi plotted against atomic mass number in (a) and condensation temperature in (b), based in part on the curve of growth shown in Fig. 3.11. Vertical boxes indicate error bars. The dotted curve in the left panel represents an $A^{-1/2}$ dependence expected for non-equilibrium accretion of gas on to grains in the ISM. The condensation temperature gives a somewhat better, though not perfect, fit, suggesting condensation under near-equilibrium conditions at a variety of temperatures either in stellar ejecta or in some nebular environment. Note the extreme depletion of Ca ('Calcium in the plane stays mainly in the grain'). After Spitzer and Jenkins (1975). Copyright by Annual Reviews, Inc.

dense molecular clouds give information on isotope ratios across galaxy

→ increase of ^{13}C & ^{18}O towards Galactic center indicates advanced degree of "secondary processing"

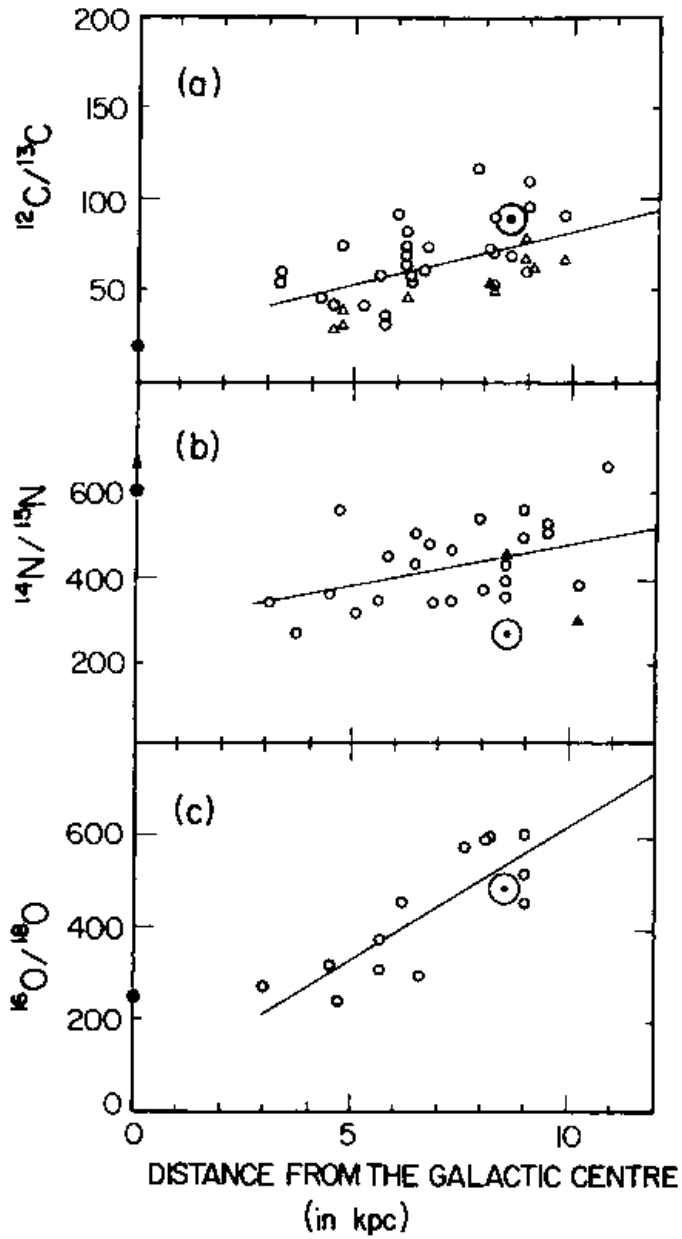

Fig. 3.43. Variation of CNO isotopic ratios with Galactocentric distance, deduced from mm wave measurements of molecules in molecular clouds. (a) $^{12}C/^{13}C$ from CO (triangles) and formaldehyde CH_2O (circles). (b) $^{14}N/^{15}N$ from HCN (circles) and NH_3 (triangles). (c) $^{16}O/^{18}O$ from formaldehyde. Solar–System values are indicated by the ⊙ sign and Galactic centre values (or a lower limit in the case of $^{14}N/^{15}N$) by a filled circle. Adapted from Wilson and Rood (1994).

- Abundances in external galaxies

most information from emission lines of H II regions + supernova remnants

also location of red giant branch in HRD:

it becomes brighter + bluer with decreasing metallicity

abundances of nearby galaxies show 2 features:

- average abundances increase with luminosity

$$\langle Z \rangle \propto L_B^{0.3} \propto M_S^{0.25}$$

$\langle Z \rangle$ luminosity-weighted mean metallicity

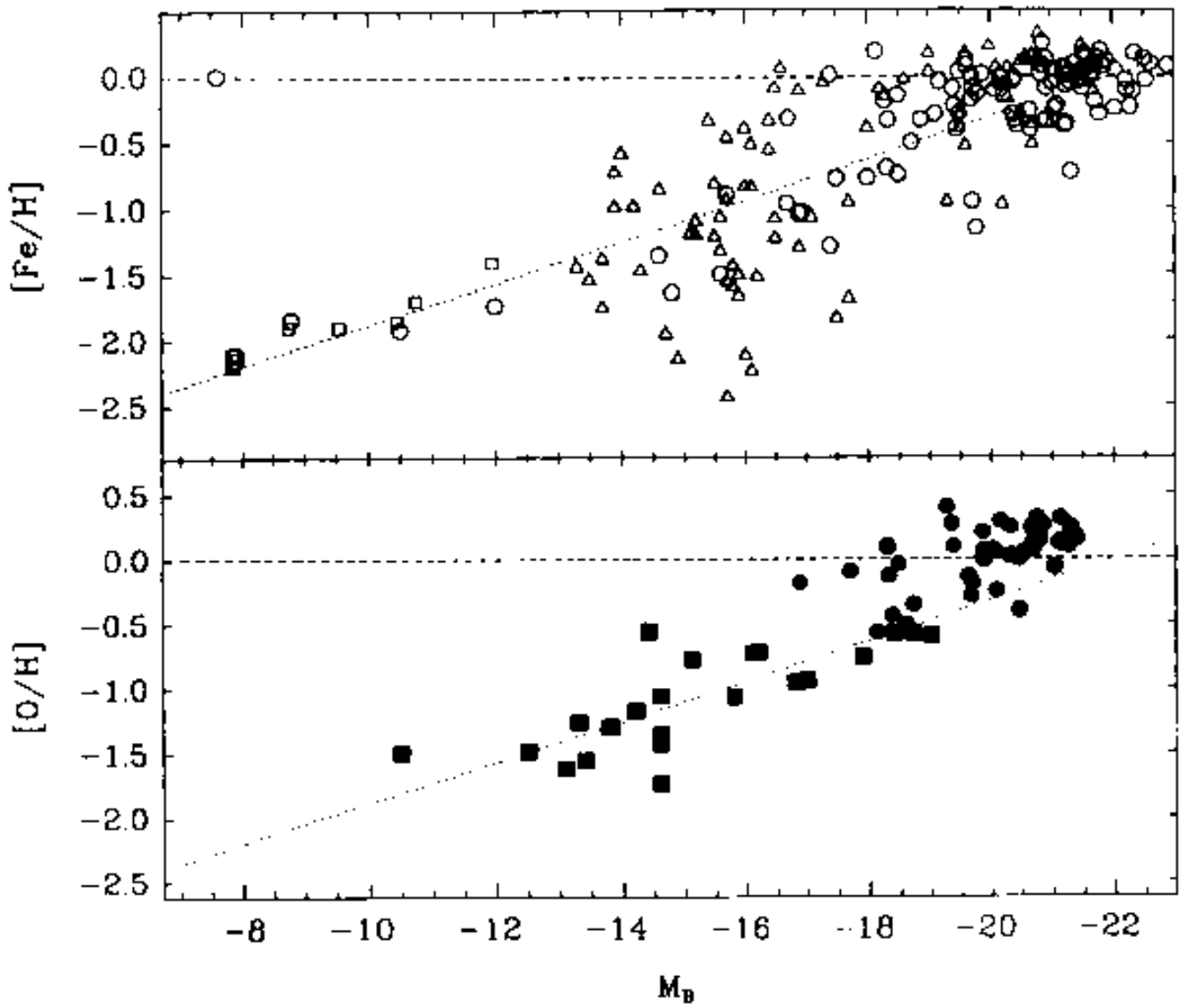

Fig. 3.44. Metallicities in gas-poor galaxies (open symbols) and oxygen abundances at a representative radius in gas-rich disk galaxies (filled symbols), as a function of galaxy luminosity in blue light. The dotted lines in each panel represent identical trends for '[Fe/H]' and [O/H] and the ordinate 0.0 represents solar composition. Adapted from Zaritsky, Kennicutt and Huchra (1994).

M_S total mass of stars + gas in galaxy

→ processed material from supernovae retained in larger gravitational potential

- most spiral + many elliptical display a large-scale abundance gradient similar to Milky-Way

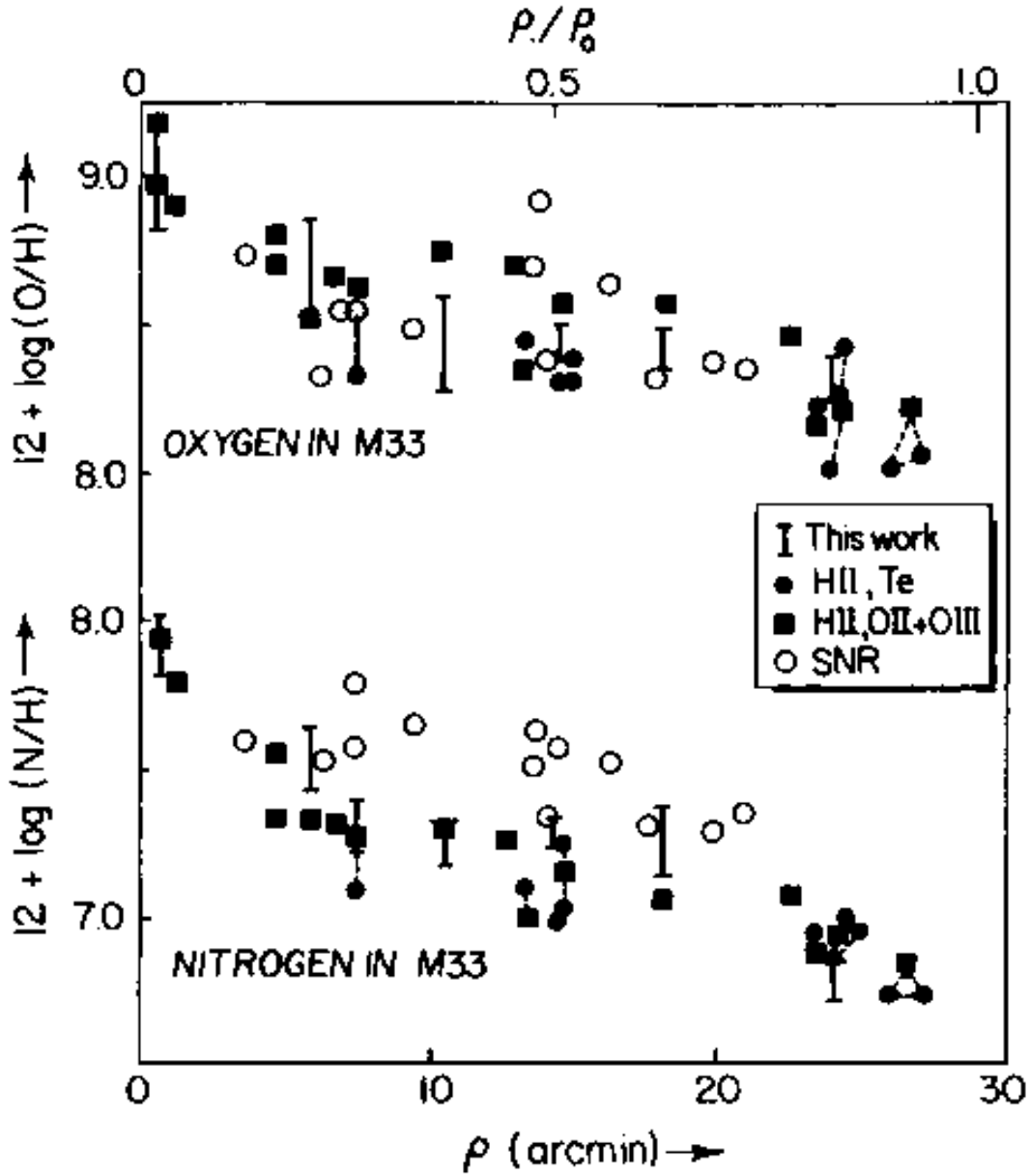

Fig. 3.45. Abundances of oxygen and nitrogen in the Scd spiral M33, measured in H II regions and supernova remnants, as a function of galactocentric distance; 1 arcmin ≡ 200 pc and ρ_0 is the de Vaucouleurs radius corresponding to a visual surface brightness of 25^m arcsec^{-2}. After Vílchez *et al.* (1988).

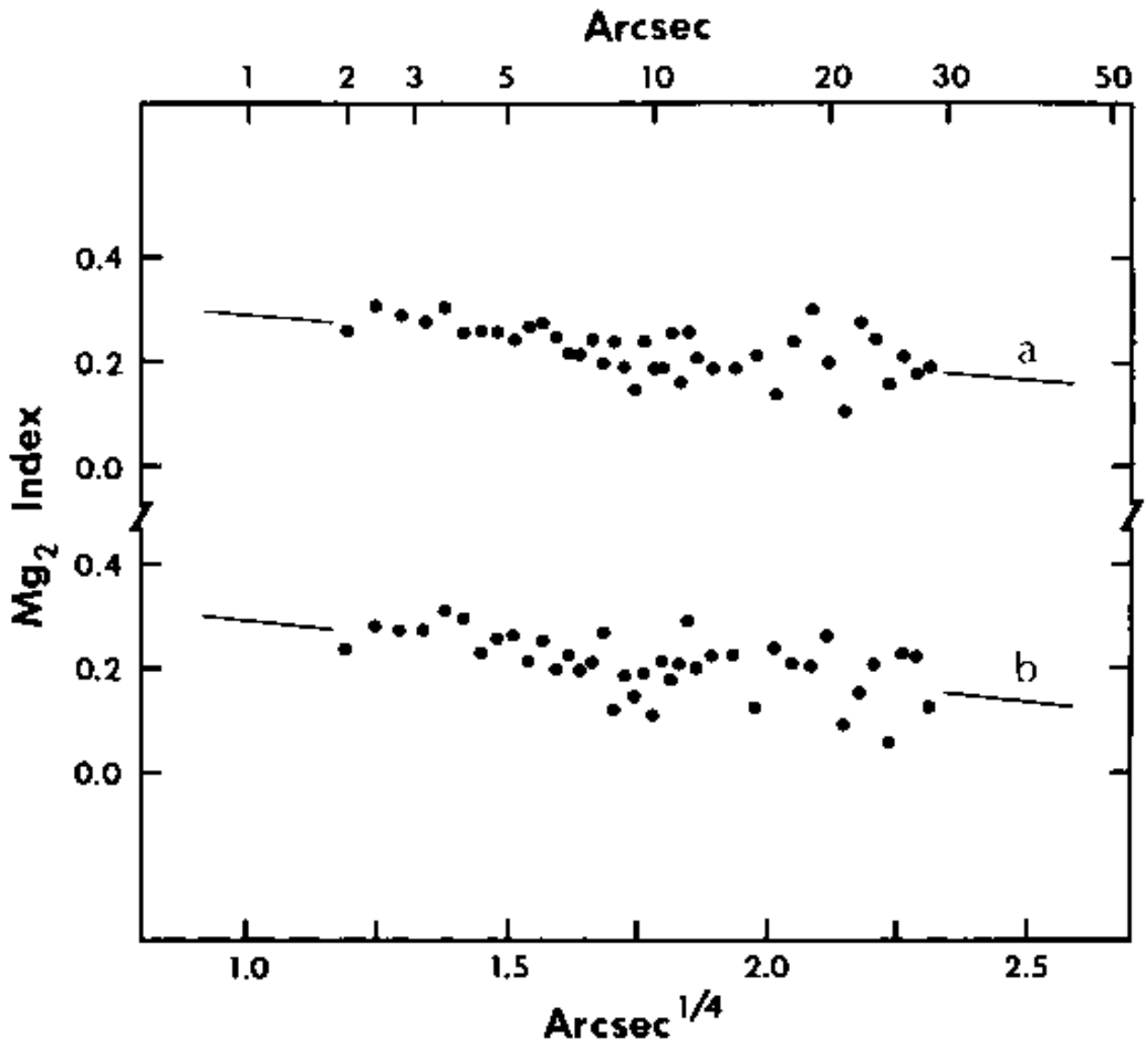

Fig. 3.46. Radial trend of Mg_2 index in the elliptical galaxy NGC 4881, after Thomsen and Baum (1987). 1 arcsec $\equiv$ 500 pc, the surface brightness in the adjoining continuum decreases from 17th to 26th magnitude per square arcsec over the range of the diagram in accordance with de Vaucouleurs' law $I \propto e^{-(r/a)^{1/4}}$ and 'a' and 'b' refer to observations taken on separate dates. Courtesy Bjarne Thomsen.